Journal of Magnetic Resonance **156,** 303–308 (2002)
doi:10.1006/jmre.2002.2566

Electron Paramagnetic Resonance Investigation of Endohedral Fullerenes N@C_{60} and N@C_{70} in a Liquid Crystal

P. Jakes,* N. Weiden,* R.-A. Eichel,* A. Gembus,* K.-P. Dinse,*,[1] C. Meyer,† W. Harneit,† and A. Weidinger†

*Phys. Chem. III, TU Darmstadt, Petersenstr. 20, D-64287 Darmstadt, Germany; and †Hahn-Meitner-Institut Berlin, Glienickerstr. 100, D-14109 Berlin, Germany

Received March 6, 2002; revised May 14, 2002

Endohedral fullerenes N@C_{60} and N@C_{70} were dissolved in the liquid crystal 4-methoxybenzylidene-4′-*n*-butylaniline (MBBA) and investigated by electron paramagnetic resonance. In both cases well resolved EPR spectra give proof for molecular orientation in the nematic mesophase. Spectral features are dominated by a nonvanishing zero-field interaction, indicating a deviation from spherical spin density distribution at the encased nitrogen atom. In N@C_{70}, a maximum order parameter $O_{33} = 0.18(3)$, correlated with the long axis of the cage, and a zero-field-splitting parameter $D = -2.6(4)$ MHz were determined. A persistent zero-field splitting is also observed in C_{60} via the quartet spin of the encapsulated nitrogen, although no assignment of the director with respect to the molecular frame is possible. The observed line splitting is indicative of pseudo orientation of the rapidly rotating cage in this case.

Key Words: **endohedral fullerene; EPR; liquid crystal; chemical trap; zero-field splitting.**

INTRODUCTION

Nonspherical molecules can be geometrically aligned by embedding them in liquid crystals (LC) which have a preferred orientation axis in an external field. Such an alignment of molecules can be extremely useful because elements of second-rank tensor interactions like dipolar coupling, nuclear quadrupole interaction (nqi), or fine structure interaction (FS) can be determined with liquid solution-like spectral resolution (*1, 2*).

A further aspect of such investigations is the study of solute/solvent interactions which are responsible for molecular alignment in uniaxial nematic mesophases. Modelling such interactions is a prerequisite for predicting molecular alignment under more general nonisotropic conditions like membranes or nanostructured matrices. Current accepted theories describe the order parameter O_{33} of a solute molecule in terms of a long-range and a short-range potential, the former being modelled as product of a time averaged electric field gradient (EFG) at the solute site and the molecular quadrupole moment of the solute molecule. The short-range term is described as a "hard sphere" potential between solute and the nematogenic solvent cage. Tests of this model were performed by using LC with an EFG vanishing at the solute site ("magic mixtures") or by studying probe molecules with zero molecular quadrupole moment ("magic solutes") in order to cancel the contribution from the long-range electrostatic potential. Predicted order parameters were in quite good agreement with experimental values thus confirming the choice of parameters for the short-range potential (*3*).

As was shown quite early, noble gas atoms could also be oriented in LC (*4*). The degree of orientation was measured by using the nuclear quadrupole moment as sensor for the local EFG, which is created by the oriented solvent molecules. Later studies of Ne, Kr, and Xe dissolved in various LC presented evidence that experimental data can only be explained by considering an additional "local" contribution to the EFG, which results from a deformed atomic charge distribution. This deformation is thought to originate from orbital "squeezing" by the nonspherical solvent cage (*5*).

In this context it was tempting to investigate the possibility to orient fullerenes in nematic mesophases, using the quartet electronic spin ($S = 3/2$) of encased nitrogen atoms as sensor which, however, is not directly coupled to an EFG. Two different cages, [D_{5h}]-C_{70} and [I_h]-C_{60} were studied, the former cage clearly being subject to orientation by long-range as well as short-range forces. The latter, with vanishing molecular quadrupole moment and an isotropic polarizability tensor, is testing exclusively fullerene cage deformations induced by the solvent cage in analogy to previous NMR studies of noble gas atoms in LC. Such symmetry lowering of the fullerene cage is detected indirectly via lifting of spherical symmetry of the spin distribution of the encased atom.

As was shown previously, supra molecules formed by nitrogen encapsulated in C_{60} or C_{70} have exceptional properties in the sense that open shell and therefore highly reactive atoms are stabilized in the center with no binding or charge transfer to the cage (*6–8*). The almost perfect shielding from the outside of the enclosed atoms gives rise to extremely sharp EPR lines and, most importantly, to long electron spin relaxation times (*7*), which are important for applications, e.g., in connection with quantum computing. In such proposals endohedral fullerenes are envisaged to serve as quantum bit carriers (*9*). Furthermore

[1] To whom correspondence should be addressed. E-mail: dinse@chemie.tu-darmstadt.de.

1090-7807/02 $35.00

it was suggested to use C_{60} dimers with nitrogen encapsulated in both C_{60} cages, the dipole–dipole interaction serving as adjustable coupling between the enclosed paramagnetic atoms to provide the necessary entanglement of the paramagnetic states. It is obvious that a control of the interaction angle is necessary if a well defined and changeable interaction is to be established. The embedding of the endohedral fullerenes in a LC matrix could provide one possible solution of this requirement (*10*).

EXPERIMENTAL

The endohedral fullerenes are produced by ion implantation (*11*). The as-prepared material is highly diluted (concentration ca. 10^{-4}) but can be enriched by HPLC chromatography (*12*). In the present experiment, as-prepared or slightly enriched (up to a factor of ten) material was used. The fullerenes were dissolved at room temperature in the LC 4-methoxybenzylidene-4′-*n*-butylaniline (MBBA) in an ultrasonic bath. A surplus of fullerenes was added in order to obtain a saturated mixture which was then decanted after the surplus fullerenes had sedimented at the bottom. Finally, the samples were degassed on a high-vacuum line and sealed off. Fourier-transform EPR (FT-EPR) measurements yielding spectra and relaxation times were performed with a Bruker ELEXSYS E 680 spectrometer at 9.5 GHz (X band).

RESULTS AND DISCUSSION

The EPR spectrum of a $S = 3/2$, $I = 1$ spin system, used to describe $N@C_{60}$ and $N@C_{70}$, consists of nine allowed transitions. Neglecting nonsecular terms of the isotropic hyperfine interaction (hfi) with the nuclear spin $I = 1$ of ^{14}N, three transitions each are frequency degenerate. Thus, a simple three-line spectrum is predicted in isotropic solution, the lines being separated by the isotropic nitrogen hfi. Second-order induced line splittings for the $|m_I| = 1$ hyperfine components (hfc) amount to 27 kHz at 0.3 T, which can be resolved under favorable conditions, because the homogeneous width of the individual transitions can be as narrow as 3 kHz. In most practical cases, however, modulation and saturation broadening contribute to an apparent degeneracy.

Under anisotropic conditions, for which the time average of the second Legendre polynomial $P_2(\Theta) = 1/2(3\cos^2(\Theta) - 1)$ is not vanishing, contributions from all traceless second-rank tensor interactions lead to energy level shifts proportional to $\langle P_2(\Theta)\rangle$. In the nematic phase, assuming nonvanishing FS of the aligned solute molecules, the degeneracy is further lifted and each hfc is visibly split in three components with an intensity ratio of 3 : 4 : 3.

For the quartet electron spin system in the nematic phase the effective spin Hamiltonian is given by (*13*)

$$\bar{H} = (g_{iso} + \bar{g})\beta_e B_z S_z + \bar{D}\left(S_z^2 - 1/3S^2\right) + (a_{iso} + \bar{a})S_z I_z. \quad [1]$$

Isotropic components of the g matrix and hyperfine coupling tensors are denoted by g_{iso} and a_{iso}, respectively. Additional terms, related to the principal component of the corresponding traceless second-rank tensor interaction, are given by

$$\begin{aligned} \bar{g} &= O_{33} g'_{zz} \\ \bar{a} &= O_{33} A'_{zz} \\ \bar{D} &= \frac{3}{2} O_{33} D'_{zz}. \end{aligned} \quad [2]$$

Here, primed values indicate components of traceless second-rank tensors of axial symmetry, and O_{33} denotes the order parameter of the solute in the nematic phase (see below). In the usual nomenclature describing the FS interaction, the zero-field-splitting (ZFS) parameter D is related to D_{zz} by $D = 2/3\, D_{zz}$.

N@C_{70} in MBBA

Because of the high symmetry of C_{70}, all matrices are of axial symmetry and furthermore a common principal axis z can be chosen. All other elements have their usual meaning. As seen from Eq. [1], only the principal elements from the traceless g-matrix as well as from hyperfine and ZFS tensors lead to spectral shifts. The z axis is taken collinear with the 3-axis, which defines the order parameter O_{33}

$$O_{33} = \frac{1}{2}(3\,\overline{\cos^2\Theta} - 1). \quad [3]$$

In a high external field (electron Zeeman interaction large compared to the hyperfine interaction), the ZFS-induced splitting $\Delta\nu$ (separation between two successive peaks in each hyperfine multiplet) in the EPR spectrum can be represented as

$$\Delta\nu = 2\mathrm{D}O_{33}. \quad [4]$$

Thus three lines are expected: one at the original position, one shifted to lower, and one to higher fields. Figure 1 shows this additional line splitting for $N@C_{70}$ in MBBA. The value for $N@C_{70}$ in the MBBA LC at 299 K is $DO_{33} = 0.418(3)$ MHz. This value was deduced from the $m_I = 0$ hyperfine component for which the splitting is not affected by a small additional shift originating from second-order hfi. The width of the center line at 299 K is 100(10) kHz, the outer lines being slightly broader by 20%. Taking this linewidth difference in account, the lines exhibit the expected intensity ratio 3 : 4 : 3.

Figure 2 shows the temperature dependence of $4DO_{33} = 6D_{zz}O_{33}$ (the splitting between the outer components) for $N@C_{70}$ in MBBA. It can be seen that the measurements performed at room temperature are close to the maximum value observed in the super-cooled nematic phase. The transition to the isotropic phase as marked by the disappearance of the splitting occurs a few degrees below the phase transition temperature of pure MBBA as reported in the literature (*14*). The depression

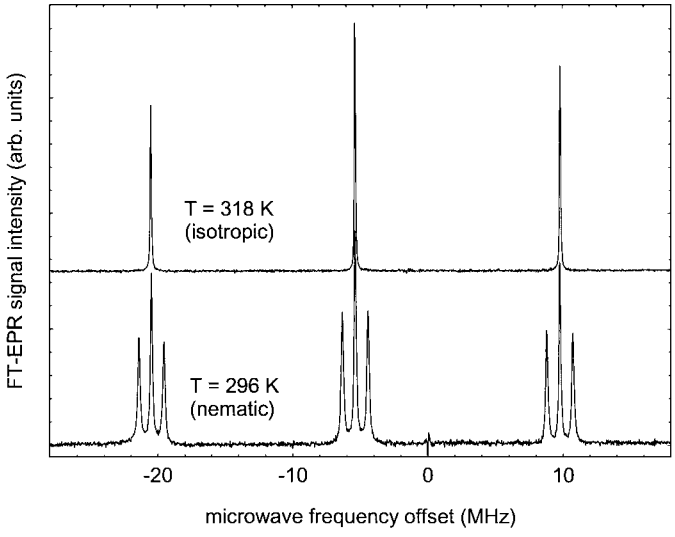

FIG. 1. EPR spectrum of N@C_{70} in the isotropic (upper graph) and nematic phase of MBBA liquid crystal (lower graph).

of the phase transition temperature might be caused by the solute present in a concentration of about 0.1 mM.

Because size and sign of the order parameter O_{33} of the solute is not known a priori, only a lower limit $|\mathrm{D}| > 0.418(3)$ MHz can be deduced from the observed maximum splitting. The sign of O_{33}, however, can be determined from the EPR spectrum by noticing that $\Delta\nu$ depends also on the nuclear spin quantum number m_I. In MBBA we find that the low frequency line triplet, which corresponds to the $m_I = -1$ hfc (assuming a positive effective hyperfine coupling constant (hfcc)), has the largest

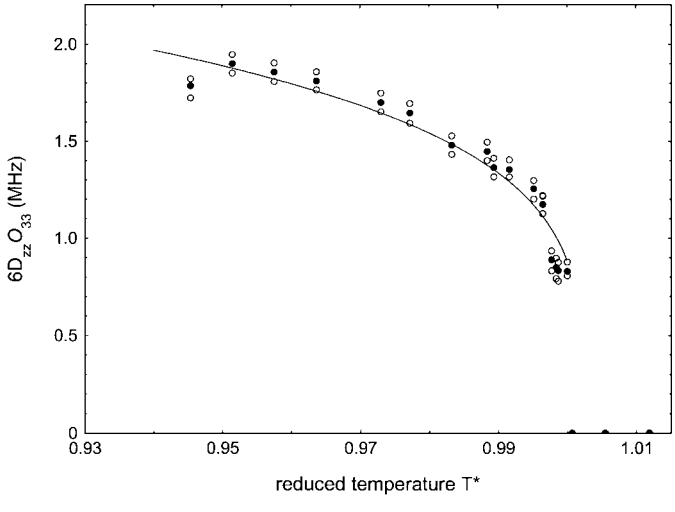

FIG. 2. Temperature dependence of $6\mathrm{D}_{zz}O_{33}$ (solid circle) of N@C_{70} in MBBA as a function of the reduced temperature $T^* = T/T_c$. These values are directly obtained by evaluating the frequency difference of the outer components of the $m_I = 0$ multiplet. Open circles denote the frequency difference measured for the $|m_I| = 1$ multiplets. The larger splitting is observed for the low frequency hfc. The data are fitted using $O_{33} \propto (1 - 0.998T^*)^{0.236}$ (see text). T_c was measured as 311.4 K.

TABLE 1

Line Positions of Allowed EPR Transitions as Function of the Effective Hyperfine Splitting a, a ZFS-induced Shift ε, and a Second-Order Shift δ (for a Definition of These Parameters See Text)

(M_S, M'_S)	$M_I = +1$ transitions	$M_I = 0$ transitions	$M_I = -1$ transitions
(3/2, 1/2)	$+a + 3\delta + \varepsilon$	$+2\delta + \varepsilon$	$-a - 1\delta + \varepsilon$
(1/2, −1/2)	$+a + 1\delta$	$+2\delta$	$-a + 1\delta$
(−1/2, −3/2)	$+a - 1\delta - \varepsilon$	$+2\delta - \varepsilon$	$-a + 3\delta - \varepsilon$

line splitting. The values for the three hfc differ by multiples of $(a_{iso} + \bar{a})^2/\nu_e = 24.5$ kHz, which can be rationalized by evaluating the energy levels of the spin system up to second-order perturbation theory. Adding nonsecular terms to the truncated Hamiltonian of Eq. [1], we obtain

$$\bar{H} = (g_{iso} + \bar{g})\beta_e B_z S_z + \bar{D}\left(S_z^2 - 1/3S^2\right) + (a_{iso} + \bar{a})S_z I_z + \frac{1}{2}(a_{iso} + \bar{a})(S_+ I_- + S_- I_+) \quad [5]$$

with "allowed" transition frequencies compiled in Table 1. Here the first-order ZFS-dependent line shifts are given in units of $\varepsilon = 3O_{33}\mathrm{D}_{zz}$ and the second-order hfi-shifts in units of $\delta = (a_{iso} + \bar{a})^2/2\nu_e$. The frequency difference of the outer line components is given as $2\varepsilon + 4\delta$, 2ε, and $2\varepsilon - 4\delta$, for $m_I = +1$, 0, and -1, respectively. For this assignment we note that the group positions are dominated by the effective hfcc $(a_{iso} + \bar{a})$, which can safely be assumed to be positive. In essence, the multiplet splitting is given either as a sum or difference of both contributions, thus allowing an unambiguous determination of the sign of $\varepsilon = 3O_{33}\mathrm{D}_{zz}$, if the sign of the dominating isotropic hfcc is known. In our case we find $\varepsilon < 0$.

For a decomposition of ε into the order parameter O_{33} and the ZFS constant D_{zz}, we use the influence of solute alignment on the nitrogen hfcc, which according to Eq. [1] modifies the isotropic hfcc by $O_{33}A'_{zz}$. In a recent ENDOR study (*15*), anisotropic hyperfine and quadrupole interactions were measured for N@C_{70} in a solid C_{70} matrix. Assuming that the low temperature value $A'_{zz} = -94(10)$ kHz (T = 80 K) can also be used to calculate the shift in the nematic phase, an effect of the order of 20 kHz is predicted, which amounts to a relative change of the effective nitrogen hfcc by only 10^{-3}. For a quantitative evaluation of $\bar{a}(T)$ one has to consider that apart from the "nematic" shift, the nitrogen hfcc is also temperature dependent with a predicted change within the nematic temperature interval by about the same amount. The detection of the predicted ordering effect therefore could accurately only be measured using FT-EPR.

In Fig. 3, the temperature dependence of the nitrogen hfcc is depicted. In the nematic phase, a decrease is detected. Assuming a positive isotropic nitrogen hfcc, a negative sign for $O_{33}A'_{zz}$ is deduced. This result is not unexpected because of the negative value of A'_{zz} (determined experimentally at 80 K (*15*)) and a predicted positive order parameter O_{33} for the elongated

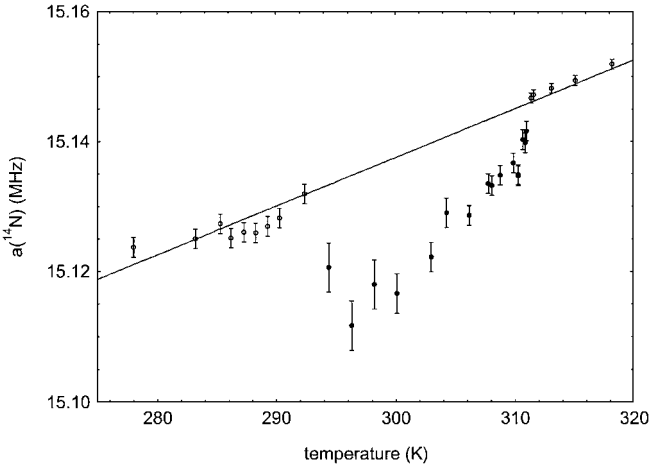

FIG. 3. Temperature dependence of the nitrogen hfcc of N@C_{70} in MBBA. Data were taken covering the polycrystalline, nematic, and isotropic phase of the solvent. The solid line is a fit of polycrystalline and isotropic data (open circles), confirming a linear temperature dependence of the isotropic hfcc in the interval studied.

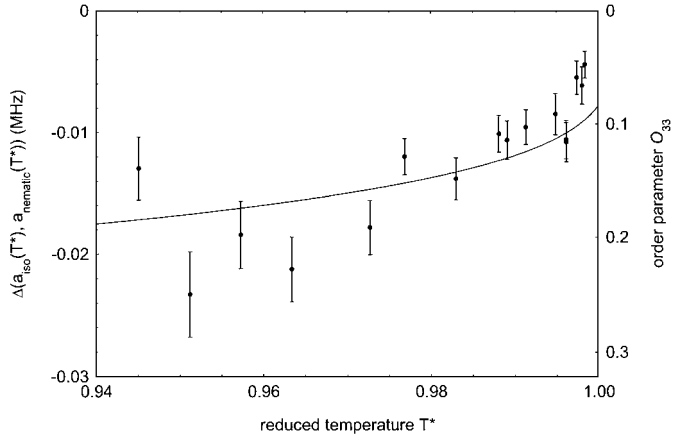

FIG. 4. Fit of the deviation of the nitrogen hfcc from its isotropic value as a function of reduced temperature. Invoking the low-temperature value of the principal value of the anisotropic hfcc, these shift values can be directly related to the order parameter of the solute.

C_{70} cage. Because of $\varepsilon < 0$ (see above), we finally conclude $D_{zz} < 0$. Considering the fact that the observed deviation from the "trivial" linear temperature dependence is not more than 20% of the linewidth of the individual components, the large scatter of data is not surprising. In order to extract a value for the order parameter O_{33} from these data, a reasonable fit could be performed only by using an analytical expression for O_{33} (T). This was obtained by fitting the ZFS-dependent multiplet splitting, which could be measured to much higher accuracy. Close to T_c, the order parameter O_{33} can be approximated by

$$O_{33} \propto (1 - bT^*)^c. \qquad [6]$$

The constants had been optimized as $b = 0.998$, $c = 0.236$ for a large set of solvent/solute systems (*5*). The reduced temperature T^* is defined as T/T_c. Using this expression, the temperature dependence of the multiplet splitting can satisfactorily be described. The applicability of this function being validated, we finally fit the hfi-dependent shift. The result is depicted in Fig. 4. Again using $A'_{zz} = -94$ kHz, the hyperfine shift can be converted into a quantitative expression for O_{33}(T) (see Fig. 4). With this quantification for O_{33}(T), we also obtain the ZFS constant (including sign) as $D = -2.3(4)$ MHz. At 293 K, $O_{33} = +0.18(3)$ is observed, still increasing slightly in the super-cooled nematic phase. In principle, the absolute value of D could also be derived from an analysis of EPR powder pattern of N@C_{70} in a C_{70} matrix at low temperatures. Attempts to measure D were unsuccessful, however, probably-because of interfering line broadening from anisotropic ^{13}C hfi, masking the expected characteristic powder pattern. We are thus lacking an independently determined value for D, which would otherwise allow us to confirm the size of the deduced order parameter O_{33}.

The observed negative sign for D might be surprising on first sight, considering the "cigarre-like" shape of the confining cage. In analogy to the arguments (*15*) used to rationalize the negative sign of A'_{zz} we note, however, that D is determined by the increase of the expectation value $\langle 1/r^3 \rangle$ of the two transverse orbitals compared to the contribution of the single parallel orbital. If all valence orbitals stay equally populated, a negative sign for D is predicted in agreement with observation.

N@C_{60} in MBBA

C_{60} has no natural axis for alignment in a LC. However, as is shown in Fig. 5 depicting the central $m_I = 0$ multiplet, the characteristic three-line pattern can also be observed for N@C_{60} in the nematic phase of MBBA. In order to enhance the visual impression of line splitting, the frequency derivative of FT-EPR derived absorption lines is shown. The line splitting

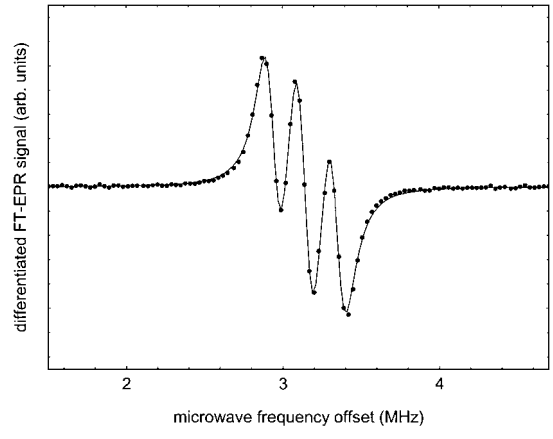

FIG. 5. Central hyperfine multiplet ($m_I = 0$) of N@C_{60} in MBBA at 295 K. The signal is derived by numerical differentiation of the FT-EPR detected absorption lines. From a fit of the multiplet, O_{33}D an be deduced.

observed at 295 K results in $D O_{33} = 0.085(2)$ MHz, about a factor of five smaller than the corresponding value for $N@C_{70}$. The linewidth (FWHM) is 200(5) kHz. Because of spectral overlap, no linewidth difference between the outer lines and the middle line could reliably be detected. The second-order hfi contribution to the multiplet splitting is slightly larger in $N@C_{60}$ than in $N@C_{70}$ (108 and 96 kHz, respectively) because of the larger nitrogen hfcc. In combination with the smaller ZFS-induced line shifts this leads to a near collapse of the high-frequency multiplet. The high frequency multiplet splitting being the smallest, we can conclude in analogy to the discussion of the $N@C_{70}$ spectra that $\varepsilon = 3 O_{33} D_{zz}$ is also negative. Lacking a reference value for A'_{zz}, no further decomposition of ε into D_{zz} and O_{33} is possible, however.

The observed splitting shows that the spin density distribution of the enclosed nitrogen atom in the nematic phase slightly deviates from spherical symmetry. As stated above, contact of C_{60} with the aligned liquid crystalline solvent cage might induce a slight deformation of the electron shell of C_{60} which in turn affects the electron density distribution of the enclosed nitrogen. In a similar experiment an EPR investigation of diluted $N@C_{60}$ in polycrystalline C_{60} below the phase transition temperature of 260 K (*8, 15*) showed a well resolved powder pattern originating from the fine structure interaction with $|D| = 0.52$ MHz. This value is approximately six times larger than $|D O_{33}|$ in the present case. Considering that most probably $|O_{33}| \ll 1$, the intrinsic D value, which represents the induced deformation of $N@C_{60}$, may well be of similar magnitude in the two cases.

It is noteworthy that the widths of EPR transitions in MBBA are significantly larger than those observed in solvents like CS_2 or toluene. This effect is not specific for the nematic phase, however. The narrowest width observed for $N@C_{70}$ in the isotropic phase of MBBA was 94 kHz (FWHM). Measuring T_1 by inversion recovery, we could confirm that this width is homogeneous. It is thus much larger than that observed in toluene at room temperature, for which $T_2 = 25\ \mu$s, corresponding to a spin packet width of only 13 kHz. A similar value is also observed for $N@C_{60}$, thus indicating that this noticeable decrease in electronic spin dephasing time has its common origin in solvent properties. As was shown previously, the dominant source of spin relaxation of $N@C_{60}$ is modulation of the FS interaction by collision-induced cage deformation. The size of this effect is determined by the variance of these fluctuations, which in turn depend of the mass of the solvent molecules. The larger width of the outer components of the resolved line triplet supports this hypothesis. Further experiments using pulse EPR techniques are in progress to derive a quantitative picture.

CONCLUSION

We have shown that $N@C_{60}$ and $N@C_{70}$ can be oriented by embedding them into LC. In case of C_{70} the alignment of the molecule is a natural consequence of its elongated shape and the molecular director can be identified as the long axis of the molecule. Furthermore, apart from its absolute size, the sign of the order parameter and of the principal ZFS tensor element could also be determined. For C_{60}, the observed anisotropy must be induced by the anisotropic LC solvent cage. As result, no unique correlation of director and cage orientation is given. In analogy to the term "pseudo rotation" used to describe Jahn–Teller induced fluctuations of the principle symmetry axis of triplet state C_{60} with respect to a given molecular frame, the observed line splitting can be related to "pseudo orientation" of the C_{60} cage. In this model, the director of cage deformation is fixed in the laboratory frame, which does not restrict fast molecular rotation. The line separation observed in the nematic phase sets a lower limit for $N@C_{60}$ as $|D| > 0.085$ MHz (see Table 2). Lacking a measured value for its order parameter, a direct comparison with $D(N@C_{70})$ is not possible. If we tentatively take as reference the value $D = 0.52$ MHz observed for $N@C_{60}$ in polycrystalline C_{60} (*16*), in which weak (van der Waals) forces from the neighboring C_{60} molecules induce the deformation, a low temperature order parameter of the order of 0.18 would result, in fortuitous coincidence with the value measured for $N@C_{70}$. Such an estimate seems to be further appropriate because the chosen reference value is much smaller than that found for externally modified fullerenes, like the mono-adduct $N@C_{61}(COOC_2H_5)_2$ (*17*) and the dimer $N@C_{60}$-C_{60} (*18*). Furthermore, as expected, the intrinsic effect from the elongated shape of the C_{70} cage would be larger than that induced externally for C_{60}.

TABLE 2

Effective ZFS Parameter $D O_{33}$ for $N@C_{60}$ and $N@C_{70}$ Measured in MBBA in Comparison with D Values Determined from EPR Powder Spectra of Immobilized Compounds. In these Experiments, Only Absolute Values of D Can Be Measured

	$\lvert D O_{33}\rvert$ (MHz)	D (MHz)	O_{33}
$N@C_{60}$ in MBBA	0.085(5)	Not determined	Not determined
$N@C_{70}$ in MBBA	0.418(3)	−2.3(4)	+0.18 (3)
$N@C_{60}$ in C_{60} ($T < 240$ K)		0.52	
$N@C_{61}(COOC_2H_5)_2$		6.2	
$N@C_{60}$-C_{60}		13.4	

A much larger FS interaction is observed for photo-excited $^3C_{60}$ in solid matrices at low temperatures, which is thought to result from a static Jahn–Teller distortion (*19*), stabilized by the crystal field. At elevated temperatures in liquid solution, EPR experiments have revealed evidence for temperature activated averaging of this interaction by interconversion between Jahn–Teller substates with differently oriented principle FS axis (*20*). Apparently, interaction with the anisotropic LC is not large enough to stabilize a specific configuration at room temperature and above. Probably for this reason, no resolved line splitting was reported when studying $^3C_{60}$ in a nematic phase (*20*). For experimental reasons it might also be difficult to observe $^3C_{70}$ with its FS tensor fixed in the molecular frame, because its homogeneous linewidth would probably be larger than 30 MHz (low

viscous solvent value), which would compete with an expected line separation of 60 MHz.

An interesting spectroscopic side effect of embedding $N@C_{60}$ and $N@C_{70}$ in the LC matrix is that the degeneracy of the transitions is lifted and therefore their properties, e.g., individual spin lattice and spin dephasing relaxation rates, can in principal be studied separately. The observed increase of the homogeneous linewidth of transitions between m_S $(-3/2, -1/2)$ and $(1/2, 3/2)$ levels relative to the central line $(-1/2, 1/2)$ is evidence for a dominant ZFS relaxation mechanism as observed previously. Its absolute size, however, is significantly larger than observed in low viscosity isotropic solvents like toluene or CS_2. Further investigations are planned for a full characterization of the relaxation mechanism.

ACKNOWLEDGMENT

Financial support from the Deutsche Forschungsgemeinschaft under Grants DI 182/22 and WE 1169/1 is gratefully acknowledged.

REFERENCES

1. H. R. Falle and G. R. Luckhurst, *J. Magn. Reson.* **3,** 161 (1970).
2. J. W. Emsley and J. C. Lindon, "NMR Spectroscopy Using Liquid Crystal Solvents," Pergamon, Oxford (1975).
3. E. E. Burnell and C. A. de Lange, *Chem. Rev.* **98,** 2359 (1998).
4. A. Loewenstein and M. Brenman, *Chem. Phys. Lett.* **58,** 435 (1978).
5. J. Jokisaari, P. Ingman, J. Lounila, O. Pulkinnen, P. Diehl, and O. Muenster, *Mol. Phys.* **78,** 41 (1993).
6. T. Almeida Murphy, T. Pawlik, A. Weidinger, M. Höhne, R. Alcala, and J. M. Spaeth, *Phys. Rev. Lett.* **77,** 1075 (1996).
7. C. Knapp, K.-P. Dinse, B. Pietzak, M. Waiblinger, and A. Weidinger, *Chem. Phys. Lett.* **272,** 433 (1997).
8. K.-P. Dinse, H. Käß, C. Knapp, and N. Weiden, *Carbon* **38,** 1635 (2000).
9. W. Harneit, M. Waiblinger, K. Lips, S. Makarov, and A. Weidinger, *AIP Conf. Proc.* **544,** 207 (2000).
10. C. Meyer, W. Harneit, K. Lips, A. Weidinger, P. Jakes, and K.-P. Dinse, *Phys. Rev.*, in press.
11. B. Pietzak, M. Waiblinger, T. Almeida Murphy, A. Weidinger, M. Höhne, E. Dietel, and A. Hirsch, *Chem. Phys. Lett.* **272,** 259 (1997).
12. A. Weidinger, M. Waiblinger, B. Pietzak, and T. Almeida Murphy, *Appl. Phys. A* **66,** 287 (1998).
13. G. Kothe, A. Naujoks, and E. Ohmes, *Mol. Phys.* **32,** 1215 (1976).
14. H. Kelker and R. Hatz, "Handbook of Liquid Crystals," Verlag Chemie, Weinheim (1980).
15. N. Weiden, B. Goedde, H. Käß, K.-P. Dinse, and M. Rohrer, *Phys. Rev. Lett.* **85,** 1544 (2000).
16. N. Weiden, H. Käss, and K.-P. Dinse, *J. Phys. Chem. B* **103,** 9826 (1999).
17. E. Dietel, A. Hirsch, B. Pietzak, M. Waiblinger, K. Lips, A. Weidinger, A. Gruss, and K.-P. Dinse, *J. Am. Chem. Soc.* **121,** 2432 (1999).
18. B. Goedde, M. Waiblinger, P. Jakes, N. Weiden, K.-P. Dinse, and A. Weidinger, *Chem. Phys. Lett.* **334,** 12 (2001).
19. G. L. Closs, P. Gautham, D. Zhang, P. J. Krusic, S. A. Hill, and E. Wasserman, *J. Phys. Chem.* **96,** 5228 (1992).
20. A. Regev, D. Gamliel, V. Meiklyar, S. Michaeli, and H. Levanon, *J. Phys. Chem.* **97,** 3671 (1993).